Available online at www.sciencedirect.com
SCIENCE DIRECT
Polymer 46 (2005) 7218–7229
polymer
www.elsevier.com/locate/polymer

Comparative deformational characteristics of poly(styrene-*b*-ethylene-*co*-butylene-*b*-styrene) thermoplastic elastomers and cross-linked natural rubber

Kishore K. Indukuri, Alan J. Lesser*

Department of Polymer Science and Engineering, Silvio O. Conte National Center for Polymer Research, University of Massachusetts, Amherst, MA, USA

Received 28 January 2005; received in revised form 27 May 2005; accepted 14 June 2005
Available online 11 July 2005

Abstract

Three poly(styrene-*b*-ethylene-*co*-butylene-*b*-styrene) (SEBS) thermoplastic elastomers (TPEs) are studied mechanically and compared to cross-linked natural rubber. It is observed that subtle alterations in the mid-block of the TPEs affect their mechanical properties significantly. The stress relaxation at room temperature is significantly altered indicating a reduced flow in systems where the ratio of ethylene to butylene segments in the mid-block is greater than one. The cyclic behavior of these systems also shows significant hysteresis. Differential scanning calorimetry suggests that these TPEs crystallize at low temperatures, similar to the observed behavior in cross-linked natural rubber. Results of internal energy changes from deformation calorimetry provide evidence for strain-induced crystallization occurring in certain SEBS systems, similar to the internal energy changes observed for cross-linked natural rubber. Simultaneous WAXD/SAXD measurements on deformed SEBS samples highlight deformation at the nanometer and the molecular length scales. In situ WAXD at different strains further reinforces the evidence for formation of strain-induced crystallites in the selected systems. Strain-induced crystallization occurring in certain TPEs provides a mechanism for reduction of flow at high strains and accounts for the retention of their highly elastic behavior.

Keywords: Strain-induced crystallization; SAXS/WAXD; Deformation calorimetry

1. Introduction

Block copolymers with a minor phase consisting of glassy or crystalline domains embedded within an elastomeric matrix are thermoplastic elastomers (TPEs) that exhibit many properties similar to those of vulcanized elastomers [1]. The deformation response of several diblock and triblock copolymer TPEs [2–7] have been studied and compared by various techniques, including small angle X-ray scattering (SAXS), transmission electron microscopy (TEM), atomic force microscopy (AFM), birefringence and rheo-optical techniques. Keller and coworkers studied highly oriented TPEs mechanically and have shown that these systems can be treated as nearly perfect composite materials [8,9]. Zhao [10] employed infra red dichroism to study the structural and morphological changes in a styrene–butadiene–styrene (SBS) block copolymer by monitoring the changes in the orientation of the polybutadiene (PB) chains on mechanical deformation. Similarly, Thomas and coworkers [11,12] studied the deformation of cylindrical PS domains of a near single crystal styrene–isoprene–styrene (SIS) triblock copolymer by SAXS and TEM techniques and related the structural changes in the hexagonal lattice of cylinders on uniaxial tensile deformation to observed macroscopic mechanical behavior. Similarly, Godovsky and coworkers [13] studied the energy and entropy effects resulting from deformation of styrene–butadiene–styrene (SBS) block copolymers and correlated the effects to structural changes in the morphology using deformation calorimetry. However, none of the block copolymer TPE systems studied for macroscopic deformation behavior possessed crystallinity and no studies have investigated morphological/structural changes that occur at both the nanometer as well as the molecular length scale (of crystalline/amorphous) on deformation.

It has been shown that by altering the ratio of ethylene to

* Corresponding author. Tel.: +1 413 577 1316; fax: 1 413 545 0082.
E-mail address: ajl@polysci.umass.edu (A.J. Lesser).

0032-3861/$ - see front matter © 2005 Elsevier Ltd. All rights reserved.
doi:10.1016/j.polymer.2005.06.025

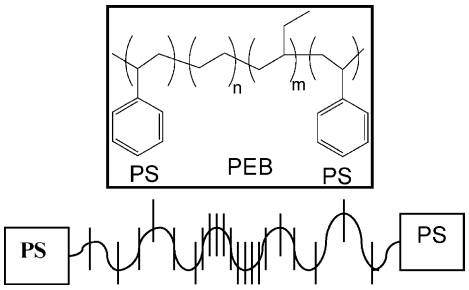

Fig. 1. (a) Structure of a typical SEBS system. (b) Structure of RP 6936 (S40E). The vertical lines in the middle block indicate the additional PS introduced into the system. The middle region has more PS than the regions close to the outer PS blocks.

butylene segments in the ethylene-*co*-butylene (EB) mid-block of the SEBS TPEs, their ability to crystallize at low temperatures can be altered [1]. Fatou and coworkers [14] have studied the thermal and mechanical properties of a series of SEBS triblock copolymers with varying % crystallinity (by changing ratio of ethylene–butylene segments) and styrene content. Gronski and Stadler [15] have synthesized elastomeric SEBS TPEs by partially hydrogenating SBS copolymers to varying degrees and studied the effects of methylene sequence length (of the EB block) on their ability to undergo strain-induced crystallization using stress relaxation experiments. They predict that stress-induced crystallization could be used as a possible mechanism to prevent flow in TPEs at high strains. However, no extensive mechanical or morphological studies have been performed on such systems.

In this paper, we present results that relate the block copolymer structure to its resulting thermal and mechanical response. In particular, the effects of the subtle changes in the mid-block architecture on the origins of elasticity and recovery are discussed. It has been shown that one critical reason for high elastic strength and recovery is associated with strain-induced crystallization similar to that observed in vulcanized natural rubber [16–22]. Internal energy measurements obtained from deformation calorimetry highlight the differences that the mid-block structure imposes on the overall mechanical properties. Also evidence that relates macroscopic deformation to deformation at different length scales has been provided through in situ SAXD/WAXD studies.

Table 1
Compositional details of the SEBS systems

Kraton (wt%)	GRP6924	GRP6926	RP6936
Simplified naming convention	S20B	S20E	S40E
Overall polystyrene %	20%	20%	40.1%
Polystyrene content in end block	20%	20%	20%

2. Experimental

2.1. Materials and sample preparation

Three poly(styrene-*b*-ethylene-*co*-butylene-*b*-styrene) (SEBS) research formulations referred to as GRP6924, GRP6926 and RP6936 and provided by KRATON polymers, US LLC were used in this study. All these three systems have the same amount of polystyrene (PS) 20% in their end blocks. GRP6924 has a ratio of ethylene to butylene segments less than one while GRP6926 and RP6936 have this ratio greater than one. RP6936 has additional styrene incorporated into the mid-block in a controlled way with more styrene present near the center than at the ends [23]. The structure of a typical SEBS triblock copolymer (a) and RP6936 (b) is shown in Fig. 1. For the sake of convenience, a simplified four letter naming convention has been adopted for these systems. The first three letters denote the total percentage of PS in the system, while the last letter denotes whether the mid-block has more number of ethylene or butylene segments. For example, system GRP 6924 with 20% PS and more butylene segments than ethylene segments is referred to as S20B. The compositions of these three systems along with the naming convention are listed in the Table 1. The three systems GRP6924, GRP6926 and RP6936 will henceforth be referred to as S20B, S20E and S40E, respectively.

Triblock copolymer samples were dissolved in toluene to obtain 3.5 wt% solutions. Solvent evaporation was controlled to occur over two weeks. The films were then dried at 40 °C under vacuum for 6 h and then annealed at 115 °C for 24 h. A natural rubber (NR) system was also used in this study and served as a reference for a chemically cross-linked elastomeric system.

2.2. Morphological characterization, thermal analysis and mechanical testing

2.2.1. Morphological characterization

Sections 40–100 nm in thickness were obtained by cyro-microtoming bulk films with a Leica EM-FCS® microtome at −90 °C. These sections were collected and then stained with ruthenium tetroxide for about 12 min. Transmission electron microscopy (TEM) studies were performed using a JEOL 2000 FX TEM operating at 200 kV. Small angle X-ray diffraction (SAXD) measurements were performed on a Molecular Metrology® SAXS machine. Wide angle X ray diffraction (WAXD) measurements were performed using a Rigaku RU-H3R rotating anode X-ray diffractometer (operating at 1.2 KW, equipped with a multilayer focusing optic: point focus (100 μm)^2; Osmic Inc., type CMF23-46Cu8) and a home built evacuated Statton-type scattering camera. Scattering patterns were acquired with a 10×15 cm^2 Fuji ST-VA image plates in conjunction with a Fuji BAS-2500 image plate scanner.

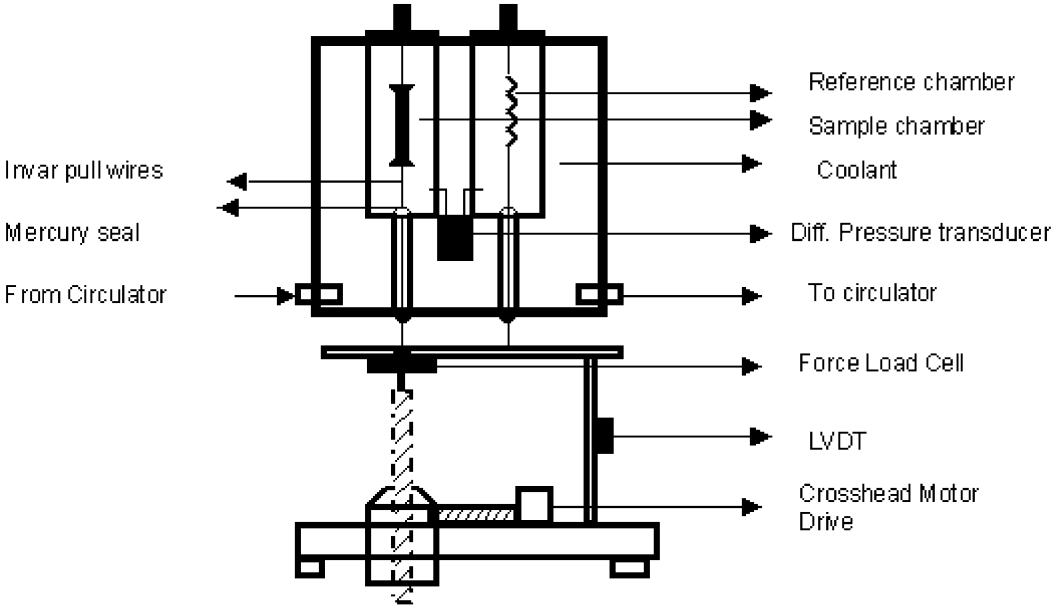

Fig. 2. Schematic of a deformation calorimeter.

2.2.2. Mechanical testing and thermal analysis

Tensile, cyclic and stress relaxation tests at different temperatures were performed on an Instron® 5800 tensile testing machine, equipped with heating/cooling stage. ASTM D1708 test geometry was employed for all the samples used for mechanical testing. Differential scanning calorimetry (DSC) and modulated differential scanning calorimetry (MDSC) were performed on a TA® Instruments Q100 DSC.

2.2.3. Simultaneous SAXS/WAXD

Simultaneous Small Angle X-ray diffraction (SAXD) and wide-angle X-ray diffraction (WAXD) under mechanical strain were performed on a molecular metrology® SAXS machine. SAXD images were calibrated using a turkey tendon standard. WAXD images were collected on a Fuji ST-VA image plate (IP) introduced in between the sample and SAXD detector. This IP has a hole in between which allows for the small angle beam to pass through and hit the SAXD detector. Reflections of tricosan and calcium carbonate samples were used to calibrate the WAXD images.

2.2.4. Deformation calorimetry

Deformation calorimetry is a technique that measures energy changes (internal energy changes, heat absorbed) on deformation and has the potential to unravel the true thermodynamic nature of the system on deformation. It has been used successfully to study the heat, internal energy changes in strain-crystallizing natural rubber [24,25], polyurethane–urea elastomers [13,26–28], thermoplastics [29] and blends [30]. The incremental work done, dW, heat

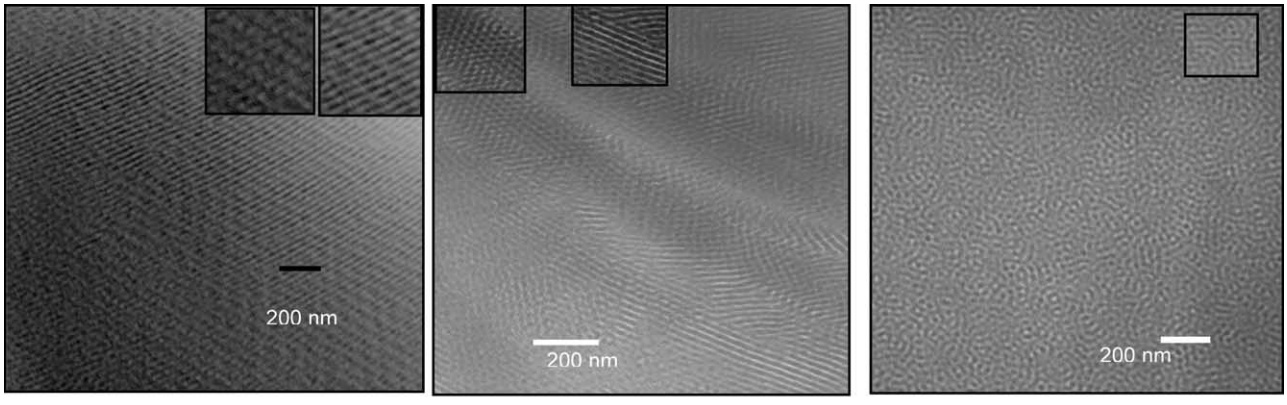

Fig. 3. Transmission electron microscopy (TEM) images of three SEBS systems.

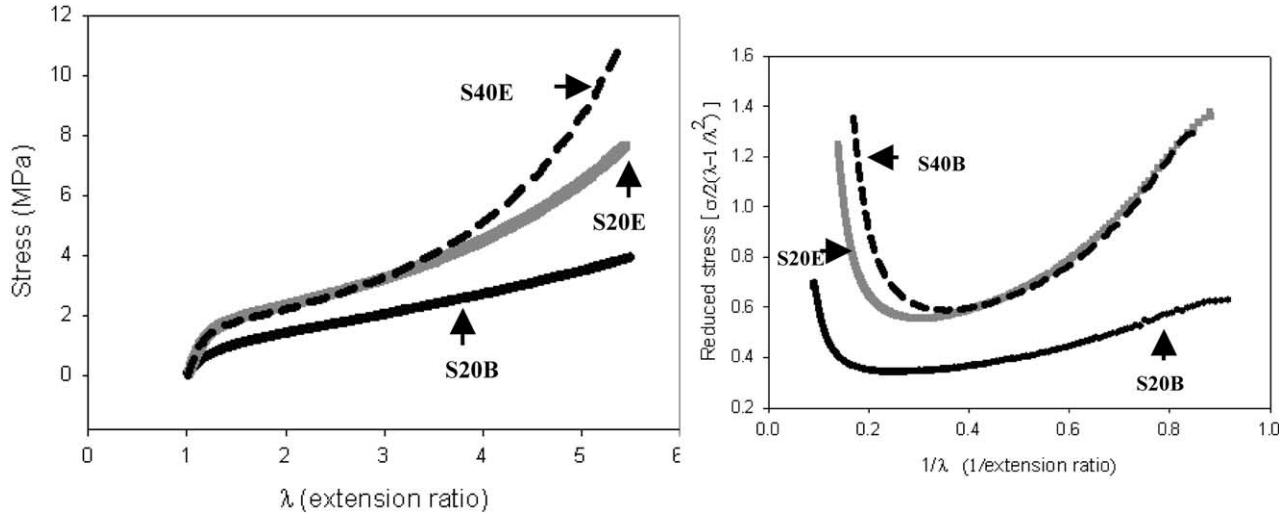

Fig. 4. Stress–extension curves for three systems and their respective Mooney Rivlin plots.

absorbed, dQ and hence the internal energy changes, dU during deformation are measured using a deformation calorimeter, which has been described previously [31,32]. Fig. 2 shows a schematic of the deformation calorimeter used in this study. This deformation calorimeter is a heat-flux device which operates on the principle of gas pressure calorimetry, where pressure changes $\Delta P(t)$, in a fixed volume of gas surrounding the source of heat (such as the sample being deformed) with respect to an identical reference cell can be related to the heat flux. The equations relating these differential pressure changes to the heat flow, dynamic heat flow have been described previously [25,31, 32]. All tests in this study were performed on an ASTM D1708 test geometry samples at a strain rate of 0.91 mm/mm/min and at 25 °C. Electrical calibrations performed yield the system constants for the calorimeter, the average time constant (for the differential pressure signal to decay or rise) and the thermal capacitance being 11.7 s and 15.24 mW/V, respectively, at 25 °C.

3. Results and discussion

Investigation of S20B, S20E and S40E by TEM, (Fig. 3) shows the same overall morphology. The PS domains coalesce into cylindrical rods that are packed in a two-dimensional hexagonal lattice embedded within the poly(-ethylene-*co*-butylene) (PEB) matrix. This is expected as all these three systems have same amount of PS (20%) in their end-blocks. This is also in accordance with what is expected from the triblock copolymer phase diagram for a 15–35% volume fraction PS system. Small angle X-ray scattering (SAXS) on these systems confirms hexagonal packing of PS cylinders in a PEB matrix. The inter-cylinder *d*-spacings for S20B, S20E and S40E have been calculated to be 25.8, 26.1 and 29 nm, respectively.

Stress-extension ratio curves for the three systems (Fig. 4) demonstrate that subtle changes in the mid-block architecture have a significant effect on the uniaxial tensile response. Both the initial strain response (low strain regime)

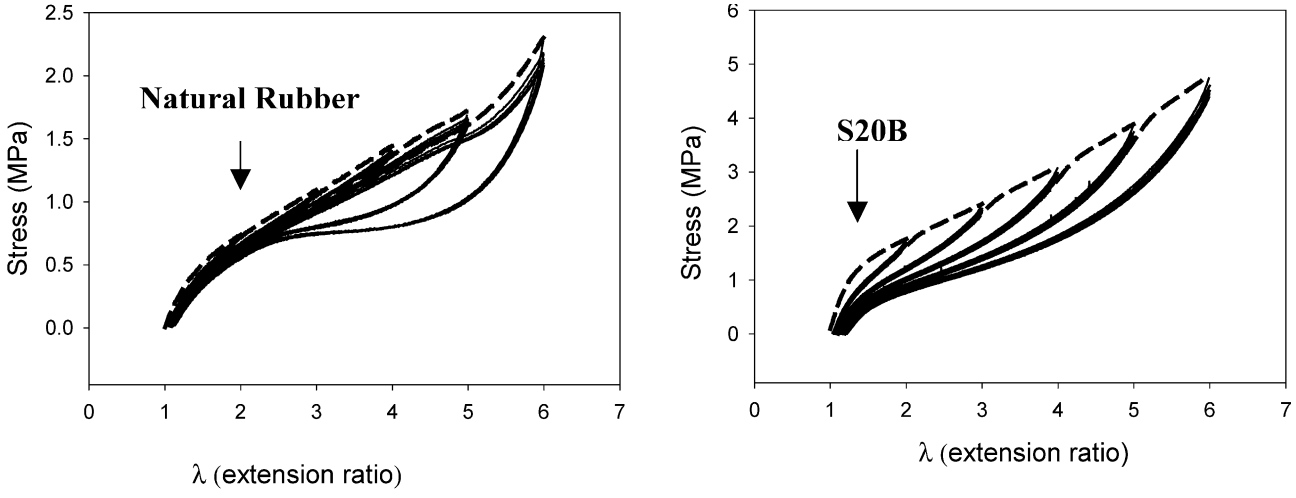

Fig. 5. Cyclic loading and unloading curves for natural rubber and S20B.

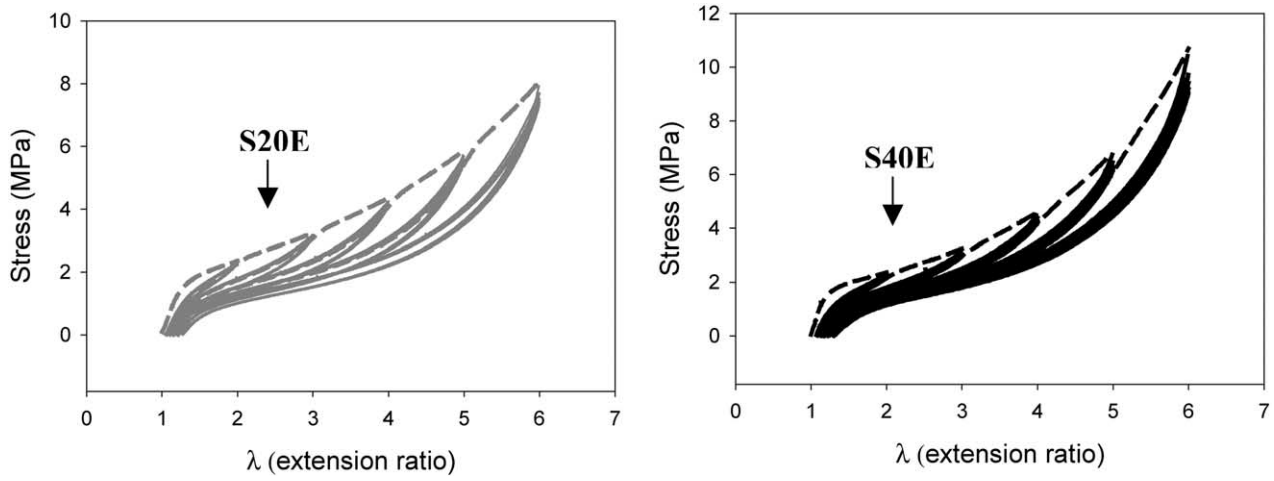

Fig. 6. Loading and unloading curves for S20E and S40E.

as well as the strain hardening behavior (large strain response) are significantly different. Note that the modulus of S20E is significantly higher than that of S20B. Thus there appears to be a direct correlation between the increase in the ratio of ethylene to the butylene segments in the EB mid-block and the modulus of the SEBS systems. Conversely, the extensibility of S20E becomes lower compared to that of S20B, indicating a reverse relationship. The higher modulus and lower extensibility of S40E compared to the other systems could be due to the additional glassy PS incorporated into the middle block for this system. The reduced stress versus inverse extension ratio plot (on the right) emphasizes this difference in behavior for the three systems.

Cyclic tests were also performed on these samples, with each sample cycled five times after an initial stretch. The initial stretch (which conditions the system for Mullin's effect) has been indicated in the corresponding Figs. 5 and 6 with a dotted line to differentiate from the consecutive loading and unloading cycles. For natural rubber (NR), it can be seen from Fig. 5 (left) that the hysteresis is almost negligible up to an extension ratio of 4. However, on further straining NR to extension ratios of 5 and beyond produces pronounced hysteresis. This hysteresis vanishes when the sample is unloaded back to an extension ratio of 2.5. This behavior has been widely attributed to strain induced crystallization that occurs in natural rubber [33].

Fig. 5 (right) shows the cyclic behavior of S20B. The initial stretch cycle resembles a thermoplastic like response (this initial stretch cycle has been shown in dotted line for clarity). However, after its initial stretch, the system behaves like a typical elastomer with a relatively low amount of hysteresis. Fig. 6 (left) also shows that S20E loads initially like a thermoplastic (indicated by dotted line) and then on subsequent cycling follows an elastomeric behavior. However, S20E shows significant hysteresis. Fig. 6 (right) shows that S40E behaves similar to that observed for S20E, but with a much lower hysteresis.

Although hysteresis in elastomers can be produced by a number of different phenomena, one such phenomenon is strain-induced crystallization. If strain-induced

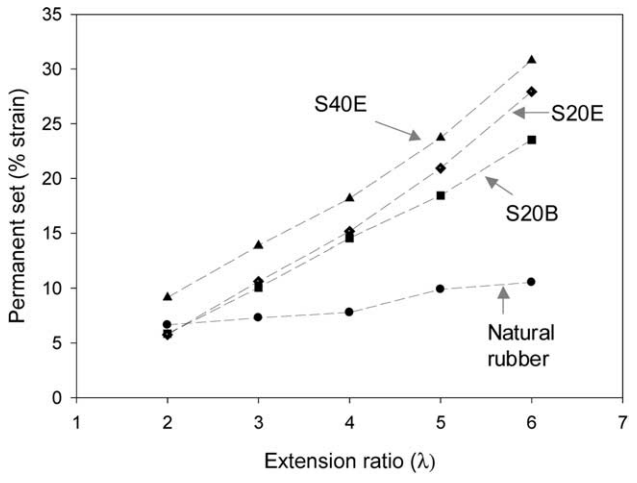

Fig. 7. Permanent set at the end of each extension cycle in cyclic tests.

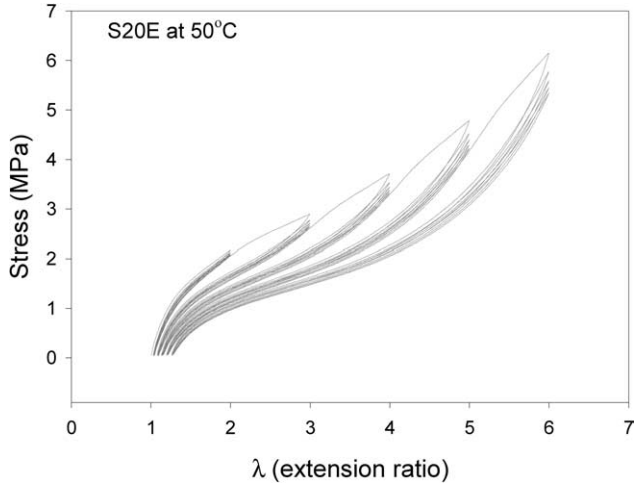

Fig. 8. Cyclic stress–strain curves for S20E at 50 °C.

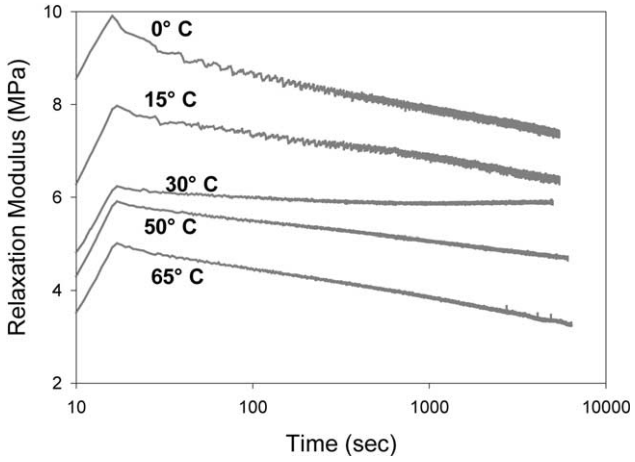

Fig. 9. Stress relaxation of S20B at 25% strain for different temperatures.

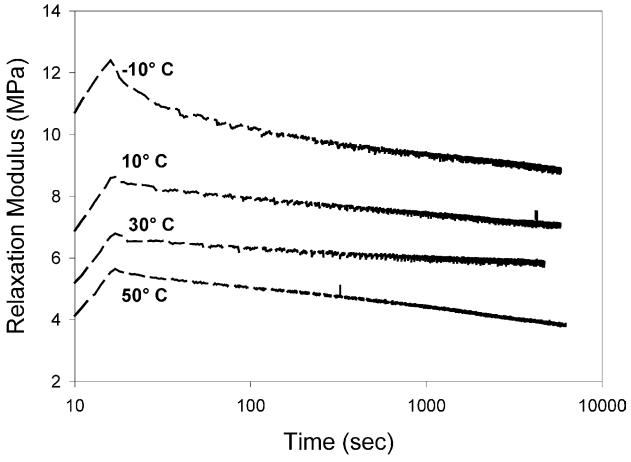

Fig. 11. Stress relaxation behavior of S40E at 25% strain for different temperatures.

crystallization is the cause for the observed hysteresis in TPEs, then the results would suggest that S20B contains no strain-induced crystals, while S20E does and S40E, a lower amount than S20E.

Fig. 7 shows the permanent set of each system after being cycled to higher extensions. S20B and S20E show the same level of permanent set to extension ratios of 4, after which the set for S20E increases slightly. It can also be seen that S40E has a higher permanent set than the other two compositions. This can be expected because S40E has higher % of glassy PS than S20B and S20E. Natural rubber in comparison shows very little permanent set and does not change much on cycling to higher extensions.

Again, taking a cue from work done on natural rubber [33], cyclic tests at different temperatures were performed on system S20E to further investigate the heterogeneity causing hysteresis. Fig. 8 shows the cyclic stress strain behavior of S20E at 50 °C. Performing cyclic tests at elevated temperatures for S20E, it is observed that as the temperature increases from 25 to 50 °C, the observed

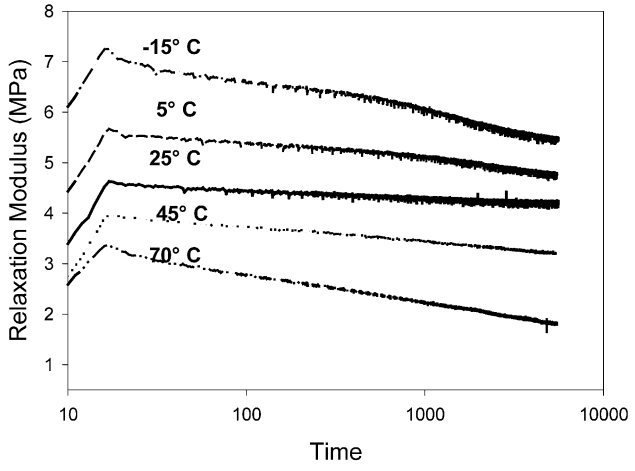

Fig. 10. Stress relaxation behavior of S20E at 25% strain for different temperatures.

hysteresis disappears (for loading–unloading cycles after its initial stretch to condition for Mullin's effect). It can be suggested that the stress-induced crystals formed at room temperatures melt on heating to 50 °C and hence the heterogeneity disappears resulting in no hysteresis. This behavior is similar to that reported for natural rubber where the hysteresis loops observed at room temperatures show a progressive diminution with rising temperature [33,34].

Stress relaxation tests at different temperatures provide important information about the nature of physical and chemical relaxation processes occurring in a material. Also stress relaxation tests have been effectively used in studying strain-induced crystallization in cross-linked natural rubber [16,17,35]. In order to probe these characteristics in SEBS materials, stress relaxations at different temperatures were performed. Figs. 9–11 show the relaxation modulus of S20B, S20E and S40E with time at different temperatures. The temperatures chosen lie between the glass transition of the elastomer phase and the glass transition of the glassy PS phase. At temperatures below room temperature, all three systems show similar stress relaxation behavior. At temperatures above room temperature (25 °C) and approaching the glass transition temperatures of PS (100 °C), significant relaxation in stress is observed and is attributed to the enhanced mobility of the PS phase. The most interesting behavior can be seen for S20E at room temperature in Fig. 10, where there is little or no stress relaxation. It should be pointed out that all stress relaxation experiments here were done by first equilibrating the samples at specified temperatures and desired strain was subsequently applied. In such an experiment, if any strain-induced crystallization occurs in the system, it would occur concurrently with stretching. Thus, stress relaxation behavior observed could be due to a combination of two effects, one due to the tendency to further crystallize leading to reduction in stress and other due to an increase in the number of effective junction points leading to an increase in stress [33]. These results in combination with the cyclic test

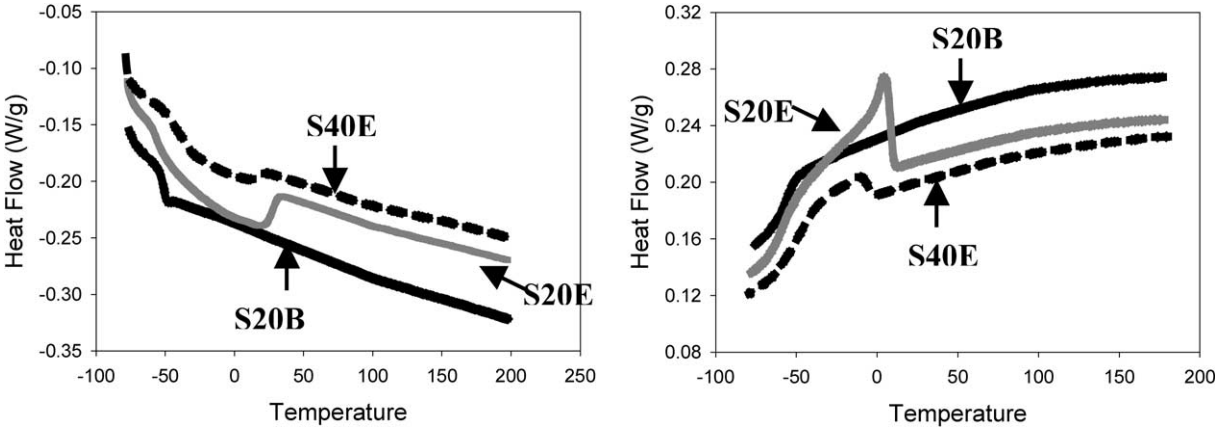

Fig. 12. Heating and cooling scans of three SEBS systems.

Table 2
% Crystallinity (heating cycle)

Kraton	Glass transition, T_g (°C)	Approx. melting temperature (°C)	% Crystallinity (corrected for PS end blocks)
S20B	−50	–	–
S20E	−55	23	15%
S40E	−34	10	6%

data suggest that there may be the formation of strain-induced crystals in the system S20E.

In order to probe the ability of these systems to crystallize thermally, Differential scanning calorimetry (DSC) studies were done. Fig. 12 shows the DSC heating and cooling scans of SEBS systems. The measured glass transition temperatures (T_g) are −55 °C for both S20B and S20E and −34 °C for S40E. This increase in T_g can be expected for S40E as it contains additional PS in the mid-block that raises the T_g of the elastomeric phase. S20E also shows a broad endotherm ranging from −40 to 30 °C, in addition to a T_g at −55 °C. This could be due to the melting of small crystals of varying size or thickness present in S20E. On following the cooling scan for S20E, the crystallization exotherm ranging from −40 to +10 °C can be observed. Such broad endotherms have been reported in the literature for other EB based block copolymer systems [14,36]. However, the endotherms observed here do not change with the sample preparation procedure as has been observed for some Poly (EBEE) block copolymer systems [36]. The system S20E with higher number of ethylene than butylene segments shows this broad endotherm, suggesting that as the number of ethylene like sequences increases, its ability to crystallize increases. S20B on the other hand does not show any melting or crystallization endotherms in the heating and cooling scans, respectively. The greater number of butylene segments in this system introduce large number of branches/defects and hinders the system from ordering/crystallizing. S40E shows melting/crystallization behavior similar to S20E, but the behavior is much less pronounced than S20E. This can be explained on the basis that even though there are more ethylene segments than butylene segments, the achievable crystallinity is further frustrated by the incorporation of additional styrene in EB mid-block of S40E. It can also be observed that the broad melting endotherms in S20E and S40E overlap with glass transition endotherms.

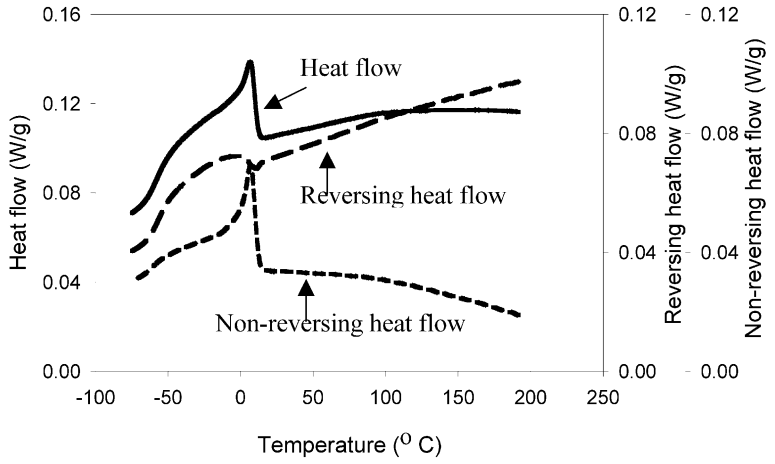

Fig. 13. Modulated DSC of cooling scans for S20E.

Table 3
% Crystallinity (cooling cycle)

Kraton	Glass transition, T_g (°C)	Approx. crystallization temperature (°C)	% Crystallinity (corrected for PS end blocks)
S20B	−50	–	
S20E	−55	7	14%
S40E	−34	−3	5%

In order to deconvolute the glass transition behavior from the melting endotherm, Modulated DSC was employed. Using this technique, the heat flow can be deconvoluted to give the thermodynamic and kinetic components of the heat flow. This is obtained by superimposing a modulated heating rate ±0.45 °C for every 60 s on top of a constant ramp rate. Fig. 13 shows the modulated DSC cooling scan of S20E. From the reversing heat flow component, T_g information can be accurately determined. Tables 2 and 3 list the % crystallinity and the crystallization temperatures for three systems calculated from MDSC heating and cooling scans, respectively. The DSC measurements clearly show low-temperature melting/crystallization behavior for systems S20E and S40E. There is evidence for the presence of small crystallites, but all these crystallites melt below room temperature. Again, this low temperature melting and crystallization behavior is similar to that observed in natural rubber [33].

WAXD measurements were performed on these three systems at room temperature to verify the DSC experiments. Fig. 14 and Table 4 shows the WAXD intensities and full width at half maximum (FWHM) of the reflections for these three SEBS systems at room temperature. These measurements show sharp amorphous halos without any crystal reflections for all the three systems. But it can be observed that the FWHM for the amorphous halos of systems S20E and S40E are smaller compared to that of S20B and suggest their ability to order and crystallize. But this does not explain the elastic hysteresis and stress relaxation behavior of S20E. Both stress relaxation and elastic hysteresis occur when the sample is stretched or strained. Natural rubber provides an excellent example of an elastomeric system, which exhibits low temperature melting/crystallization behavior, shows no crystallinity at room temperature but crystallizes on stretching it to 400% strain.

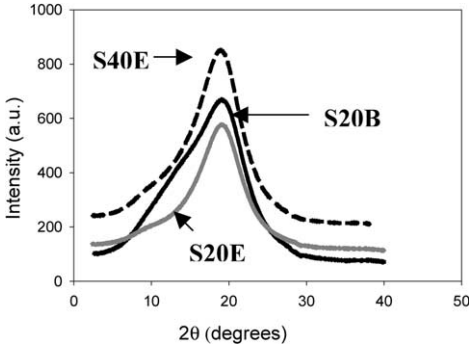

Fig. 14. WAXD intensities for three SEBS systems at room temperature.

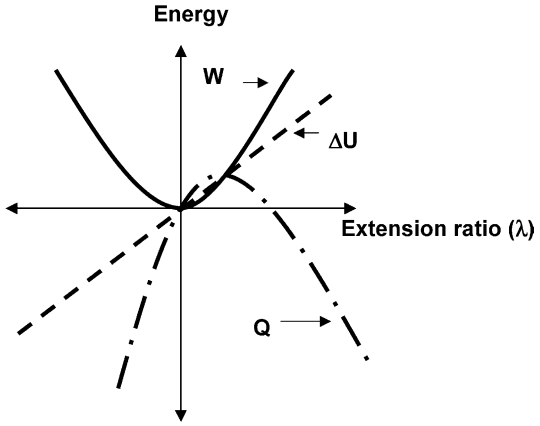

Fig. 15. Heat, Q, work, W and internal energy change, ΔU for a linear rubbery solid for small strains.

In order to study the ability of these systems to undergo strain-induced crystallization, deformation calorimetry studies were performed. Fig. 15 displays the heat Q, work, W and internal energy change, ΔU for an ideal linear rubbery solid for small strains. Non-linear effects like strain-induced crystallization, strain induced phase mixing in two-phase TPEs, hydrogen bonding etc. affect this ideal behavior in elastomers. Fig. 16 displays the calculated heat, work and internal energy profiles in natural rubber, normalized by the weight of the sample, as a function of the extension ratio. Stress versus extension ratio plot has been overlaid on the background for reference. As can be seen in Fig. 16 and reported elsewhere for natural rubber [25], at lower extension ratios (up to 4), the changes in internal energy are positive and rise gradually as expected for an elastomeric solid. However, on further deformation of sample above $\lambda = 4$, there is a sharp drop in internal energy, with the change in internal energy now becoming negative and dropping to about −8 J/g on reaching an extension ratio of 5.6. This drop in internal energy has been attributed [25] widely to the strain-induced crystallization occurring in natural rubber at these extension ratios. The unloading curve shows a slightly different response. There is a protracted endotherm at higher extension ratios suggesting some possible melting and recrystallization of strain-induced crystals upon unloading. The combination of these two processes during unloading delays the complete melting of strain-induced crystals to much lower extension ratios than that required to initiate crystallization during loading. It can

Table 4
FWHM of the diffraction peaks of the three systems

Polymer	Peak-mean position (2θ)	Full width at half maximum (FWHM) 2θ°
S20B	19.1	11.4
S20E	19.0	7.5
S40E	19.1	8.3

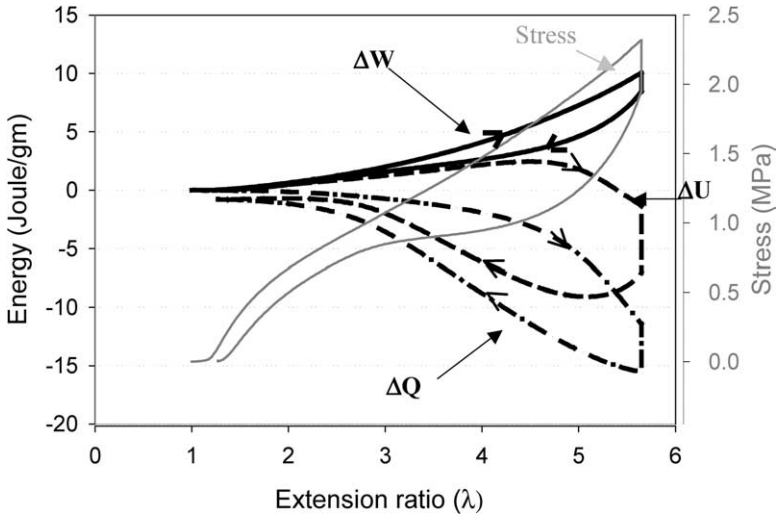

Fig. 16. Energetics of deformation of natural rubber.

also be observed that large internal changes observed at higher extension ratios are completely recoverable on unloading, suggesting that crystallization and melting occur to yield no net change in the internal energy. All these observations are in accordance with previous studies on crosslinked natural rubber [25,30,37].

From Fig. 17, it can be seen that as work done (ΔW) on the S20B system increases with increasing extension ratio, its internal energy also rises proportionately with increasing stretch and hence behaves very close to a linear rubbery solid depicted in Fig. 15. This behavior can be anticipated for S20B system from our earlier results on mechanical testing, DSC and WAXD where this system does not crystallize either thermally at low temperatures or under strain. The change in the internal energy rises upon loading the sample and drops similarly upon unloading the sample. It can be observed that the changes in internal energy and the changes in heat absorbed are not fully reversible. There is a lot of irrecoverable internal energy in the material corresponding to about 5 J/g upon unloading the sample. A residual strain of approximately 25% remains in the material upon unloading. These changes can be expected because of the deformation of glassy PS domains as the system is loaded to high extension ratios.

Fig. 18 shows the energetics of deformation of S20E. It can be immediately observed from the change in internal energy, ΔU, that this system behaves entirely different from S20B. The change in internal energy resembles that of natural rubber in that there is considerable drop in internal energy upon extension. This negative change in internal energy provides strong evidence for strain-induced crystallization in S20E similar to that observed in natural rubber. Also important differences can be observed for S20E in comparison with natural rubber. First the internal energy drop for the system S20E starts occurring at low extensions and continues to decrease on further extension. Secondly, there is a residual strain of about 35% left in the material on unloading the system. This is in agreement with

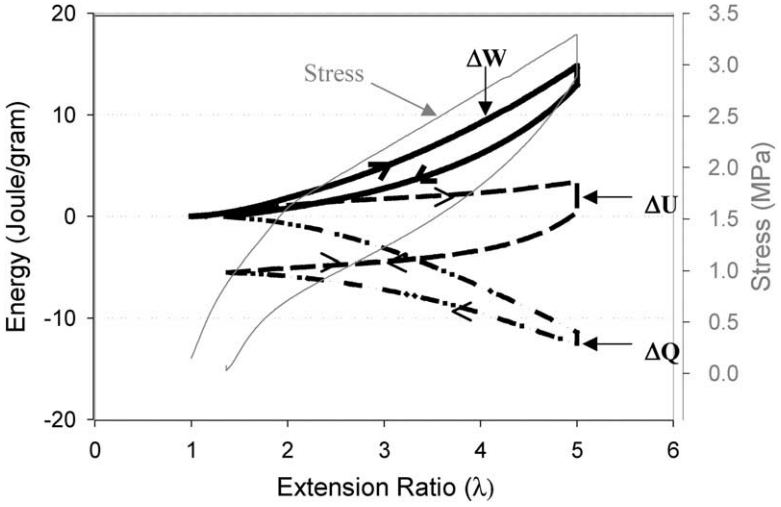

Fig. 17. Energetics of deformation of S20B.

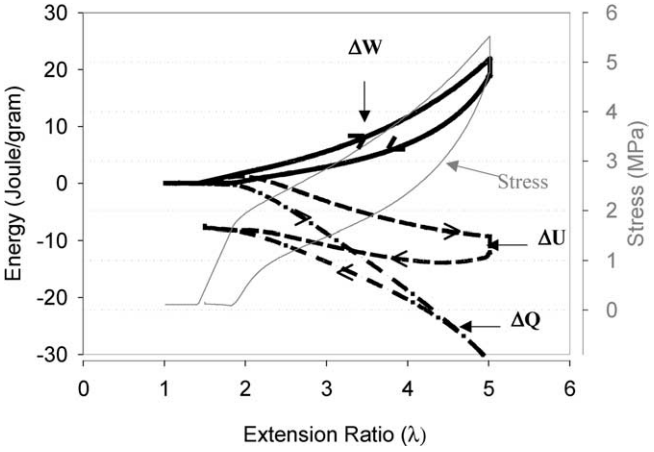

Fig. 18. Energetics of deformation of S20E.

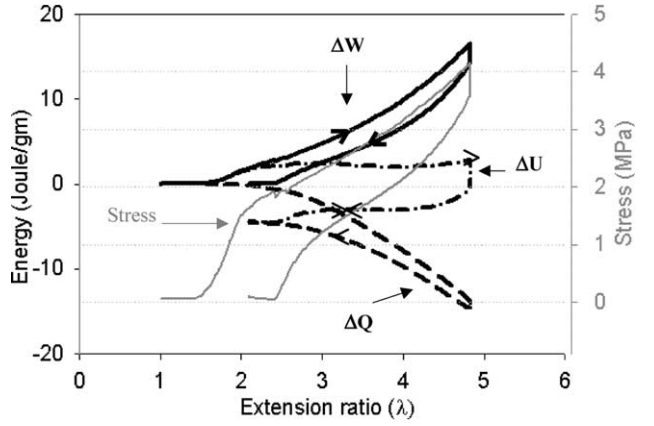

Fig. 19. Energetics of deformation of S40E.

independent permanent set data obtained from cyclic test data. Also, there is significant irrecoverable internal energy in the material as the sample is unloaded, different from completely recoverable internal energy observed for natural rubber. These changes can be expected and are due to permanent deformation of cylindrical PS domains at higher extensions. The negative internal energy changes for S20E at low extension ratios suggest that strain-induced crystallization occurs in S20E at extensions much lower compared to those at which strain-induced crystallization occurs in natural rubber. This result is in complete agreement with the results obtained from stress relaxation behavior of S20E at 25% strain. Even at such low strains, the relaxation behavior is significantly altered for S20E. Also, the cyclic test data suggests that the formation of strain-induced crystals (leading to hysteresis) occurs at lower strains and persists as the sample is strained to an extension ratio of 6. The deformation calorimetric data thus supports strain-induced crystallization at low strains for S20E. Similar results for strain-induced crystallization at lower extensions has been reported previously [25] for polyurethane–urea elastomers (with polyether soft segments) using deformation calorimetry studies.

Fig. 19 shows the energetics of deformation of S40E. As the work done on the system (ΔW) increases with stretch ratio, change in internal energy (ΔU) also rises proportionately. This behavior is similar to that observed for S20B. Until an extension ratio of 3 is reached, the internal energy rises like that of an linear elastomeric solid, but then on further extension beyond $\lambda = 3$, there is a slight drop in internal energy though the overall internal energy change still remains positive. This slight drop in internal energy suggests some strain-induced crystallization occurring in S40E, although to a much lower extent than S20E. It can be observed that this system also shows the highest residual strain of all three SEBS systems studied. This can be explained on the basis of the increased amount of PS present in the elastomeric matrix for the S40E system.

In order to further confirm the effects of strain on these SEBS systems, simultaneous WAXD and SAXD measurements were performed on these systems. WAXD/SAXD traces were collected on samples by subjecting them to different strain levels until break in a typical uniaxial tensile deformation geometry. The deformation of the PS cylinders with strain is clearly detected in the SAXD images shown in Fig. 20. The initial isotropic hexagonal lattice at zero strain distorts into an ellipsoid at lower strains and subsequently into a four-point pattern at higher strains. These structural changes in morphology of hexagonal cylinders with deformation have been studied extensively for other block copolymer systems [2–7,11,12]. A detailed analysis of SAXD patterns, along with accompanying WAXD patterns will be presented in a different publication. Fig. 21 shows

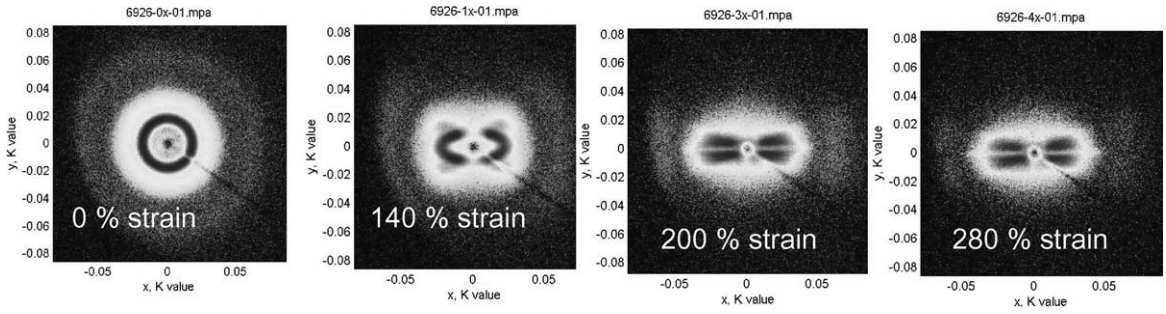

Fig. 20. SAXD diffraction images of S20E at different strains.

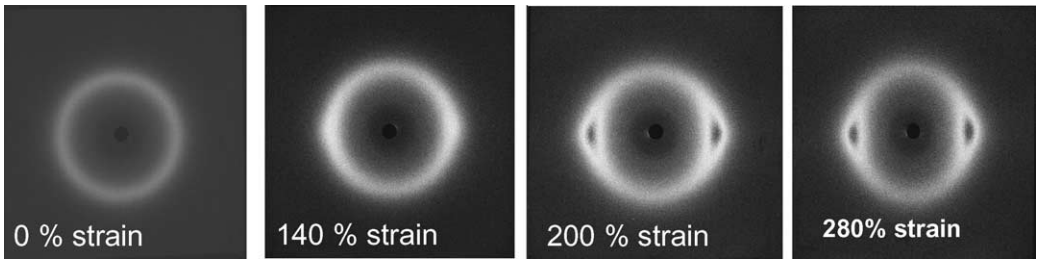

Fig. 21. WAXD at different strains for S20E.

the wide-angle diffraction images of S20E at different strain levels. As 200% strain is reached in S20E, the appearance of a bright arc is observed on top of the amorphous halo suggesting the formation of crystallites upon strain. The *d*-spacing of this reflection has been calculated to be 4.56 A^{-1}. Higher order peaks of this are not present on further straining the sample. This can be due to very small dimensions of the imperfect crystalline structures leading to lack of constructive interference for these SEBS systems. Such small crystallites giving poor constructive interference in WAXD have been reported for ethylene copolymers [38]. Fig. 22 does not show the formation of a bright arc for S20B as has been observed for S20E. Fig. 22 (right) also shows the formation of strain-induced crystals for cross-linked natural rubber at 400% strain for comparison. S40E also shows similar evidence for formation of small imperfect crystallites, but is much less pronounced than S20E. The above in situ deformation WAXD tests provide some more evidence for the formation of strain-induced crystals explaining the interesting stress relaxation and elastic hysteresis response for S20E. In situ WAXD studies on S40E also suggest some strain-induced crystallization in this system, albeit to a much lower extent than S20E and confirms the slight drop in internal energy measurements from deformation calorimetry near extension ratio of three for S40E.

4. Conclusions

Evidence for strain-induced crystallization in certain SEBS triblock copolymer TPE systems is presented and related to the interesting mechanical behavior, including reduction in flow as observed from stress relaxation tests, elastic hysteresis observed in cyclic tests. Similarities between mechanical and thermal behavior of cross-linked natural rubber and these SEBS systems have been highlighted. The low temperature melting behavior of such systems, having increased number of ethylene-like sequences, (ethylene to butylene ratio greater than one) has also been highlighted. Also, increased modulus and decreased extensibility have been accounted for on the basis of PS content, mid-block architecture and the ethylene to butylene ratio of the mid-block. Deformation calorimetry establishes the differences in internal energy behavior of these three systems and provides evidence for strain-induced crystallization occurring in systems with increased number of ethylene-like sequences. WAXD data from simultaneous SAXD/WAXD experiments provide further evidence and confirms strain-induced orientation/crystallization occurring in systems with increased ethylene-like sequences.

Acknowledgements

The authors would like to acknowledge KRATON polymers, US LLC for funding support and Dr Kathryn Wright at KRATON polymers, US LLC for her helpful suggestions. We would also like to acknowledge Prof Richard J. Farris and Prof Edward Atkins for valuable suggestions on deformation calorimetry and X-ray diffraction data, respectively.

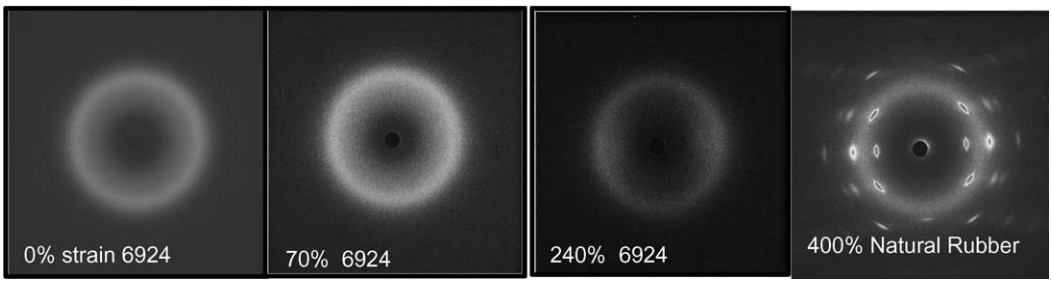

Fig. 22. WAXD diffraction images of S20B at different strains and Natural rubber at 400% strain.

References

[1] Holden G, Legge NR, Quirk R, Schroeder HE. Thermoplastic elastomers. Munich: Hanser Publishers; 1996. p. 620.
[2] Beecher JF, Marker L, Bradford RD, Aggarwal SL. J Polym Sci, Part C 1969;26:117–34.
[3] Inoue T, Masahiko M, Hashimoto T, Kawai H. Macromolecules 1971; 4:500–7.
[4] Pakula T, Saijo K, Kawai H, Hashimoto T. Macromolecules 1985;18: 1294–302.
[5] Agarwal SL. Polymer 1976;17:938–56.
[6] Huy TA, Adhikari R, Michler GH. Polymer 2003;44:1247–57.
[7] Seguela R, Prudhomme J. Macromolecules 1988;21:635–43.
[8] Arridge RGC, Folkes MJ. J Phys D: Appl Phys 1972;5:344–60.
[9] Folkes MJ, Keller A, Scalisi FP. Kolloid Z 1973;251:1–4.
[10] Zhao Y. Macromolecules 1992;25:4705–11.
[11] Honeker CC, Thomas EL, Albalak RJ, Hajduk DA, Gruner SM, Capel MC. Macromolecules 2000;33:9395–406.
[12] Honeker CC, Thomas EL. Macromolecules 2000;33:9407–17.
[13] Godovsky YK. Makromol Chem Suppl 1984;6:117–40.
[14] Sierra CA, Galan C, Fatou JG, Parellada MD, Barrio JA. Polymer 1997;38:4325–35.
[15] Stadler R, Gronski W. Colloid Polym Sci 1986;264:323–31.
[16] Gent AN. Trans Faraday Soc 1954;50:521–33.
[17] Gent AN. Rubber Chem Technol 1955;28:36–50.
[18] Luch D, Yeh GSY. J Macromol Sci, Phys 1973;7:121–55.
[19] Roberts DE, Mandelkern L. J Am Chem Soc 1955;77:781–6.
[20] Toki S, Fujimaki T, Okuyama M. Polymer 2000;41:5423–9.
[21] Trabelsi S, Albouy P-A, Rault J. Macromolecules 2003;36:7624–39.
[22] Mark JE. Polym Eng Sci 1979;19:409–13.
[23] Bening RC, Handlin JRDL, Sterna LL, Willis CL, USA Patent No. US 20030176582A1; 2003.
[24] Lyon RE, Farris RJ. Polym Eng Sci 1984;24:908–14.
[25] Lyon RE, PhD Thesis, University of Massachusetts, Amherst; 1985, p. 214.
[26] Lyon RE, Wang DX, Farris RJ, MacKnight WJ. J Appl Polym Sci 1984;29:2857–72.
[27] Godovsky YK, Bessonova NP. Colloid Polym Sci 1983;261:645–51.
[28] Godovsky YK, Bessonova NP. Thermochim Acta 1994;247:19–33.
[29] Adams GW, Farris RJ. J Polym Sci, Part B: Polym Phys 1988;26: 433–45.
[30] Agarwal N. PhD Thesis, University of Massachusetts, Amherst; 1998, p. 249.
[31] Lyon RE, Raboin PJ. J Therm Anal 1995;44:777–93.
[32] Lyon RE, Farris RJ. Rev Sci Instrum 1986;57:1640–6.
[33] Treolar LRG. The physics of rubber elasticity. Oxford: Oxford University Press; 1975. p. 324.
[34] Erman B, Mark JE. Structures and properties of rubberlike networks. Oxford: Oxford University Press; 1997. p. 370.
[35] Gent AN, Zhang L-Q. J Polym Sci, Part B: Polym Phys 2001;39: 811–7.
[36] Douzinas KC, Cohen RE, PhD Thesis, Massachusetts Institute of Technology, Cambridge; 1991, p. 382.
[37] Adams GW, PhD Thesis, University of Massachusetts, Amherst; 1987, p. 255.
[38] Mathot VBF, Scherrenberg RL, Pijpers TFJ. Polymer 1998;39: 4541–59.